Journal of Luminescence 153 (2014) 169–176

Contents lists available at ScienceDirect

Journal of Luminescence

journal homepage: www.elsevier.com/locate/jlumin

Effects of spontaneously generated coherence on resonance fluorescence from triple quantum dot molecules

Si-Cong Tian [a], Cun-Zhu Tong [a,*], Chun-Liang Wang [b], Yong-Qiang Ning [a]

[a] State Key Laboratory of Luminescence and Applications, Changchun Institute of Optics, Fine Mechanics and Physics, Chinese Academy of Sciences, Changchun 130033, China

[b] Laboratory for UV Light-Emitting Materials and Technology of Ministry of Education, Northeast Normal University, Changchun 130024, China

ARTICLE INFO

Article history:
Received 31 December 2013
Received in revised form
12 March 2014
Accepted 14 March 2014
Available online 28 March 2014

Keywords:
Triple quantum dot molecules
Electron tunneling
Resonance fluorescence
Spontaneously generated coherence

ABSTRACT

The resonance fluorescence spectrum from a triple quantum dot molecules controlled by tunneling is investigated. The positions, widths and heights of the resonance fluorescence peaks can be modified by the tunneling between the dots rather than the laser field, and interesting features such as controllable triple narrow peaks are obtained. The spectrum is explained with the transition properties of the dressed states generated by the coupling of the tunneling and the laser field. These features can also be viewed as the effects of spontaneously generated coherence between the close-lying states in the dressed state picture of the tunneling couplings, which can permit the observation of spontaneously generated coherence in quantum dot molecules.

1. Introduction

Recently much interest has been attracted by the coherent manipulation of semiconductor quantum dots (QDs) [1–5]. The research is motivated by the proposal of using QDs as the basic building block of quantum information technology, such as qubits for quantum computers [6], single photon emitters [7], all-optical quantum gate [8] and entangled-photon sources [9]. In order to reduce decoherence effects, resonant optical excitation is often employed in experiments with semiconductor QDs. For an ideal two-level system, it is well known that strong resonant excitation with a continuous wave field results in a so-called resonance fluorescence spectrum containing three peaks, known as the Mollow triplet. This iconic spectral feature was first predicted by Mollow [10] and has been demonstrated experimentally for atoms [11], single molecules [12] and self-assembled semiconductor QDs [13]. The resonance fluorescence spectrum of multiple-level system driven by two or more lasers has much more structure and shows a variety of interesting effects, duo to the more complex internal dynamics of the system [14,15].

In a quantum dots molecules (QDMs) coupled by tunneling, an external electric field allows us to control the confining potential and the number of electrons in each artificial atom, where it is possible to create a multiple-level system. Building on the vertical [16] and lateral [17] double quantum dots (DQDs) with controlled electron numbers, a triple quantum dots (TQDs) has been realized in much experimental progress [18–21]. TQDs might serve as a laboratory for correlated electron systems as well as a prototype quantum processor based on charge and/or spin in QDs [22,23]. There are other applications of TQDs in the area of quantum computation, such as quantum teleportation [24] and exchange-controlled qubit [25]. And also TQDs allows for application of tools known from quantum optics, such as the rectification [26] or the coherent electronic transfer using adiabatic passage [27].

On the other hand, the properties of resonance fluorescence spectrum can be modified by spontaneously generated coherence (SGC). SGC refers to the interference of two or more decay channels with nonorthogonal electric-dipole transition matrix elements. SGC can find applications in many fields such as quantum information and computation [28], lasing without inversion [29], all-optical switching [30], quantum photocell [31] and high-precision metrology [32]. In the presence of SGC, the spectrum of resonance fluorescence can be demonstrated to exhibit narrowing [33], quenching [34], squeezing [35] and superfluorescence [36]. But the existence of SGC requires two stringent conditions: the close-lying levels are near degenerate and the corresponding dipole transitions are not orthogonal. These conditions are very difficult to be fulfilled in real systems. As a result, there are hardly any direct experimental observations on the phenomena related to SGC.

In this paper, we investigate the resonance fluorescence spectrum from TQDs. By changing the tunneling between the TQDs, the

* Corresponding author.
E-mail address: tongcz@ciomp.ac.cn (C.-Z. Tong).

http://dx.doi.org/10.1016/j.jlumin.2014.03.034
0022-2313/

positions, linewidths and heights of the fluorescence peaks can be controlled. Interesting features, such as triple narrow lines in the resonance fluorescence spectrum is obtained. Unlike the atomic system, in TQDs we can use tunneling instead of laser field to create the necessary coherence. We explain the phenomena in the dressed state basis of the laser field and the tunneling couplings. On the other hand, in the dressed state basis of the two tunneling couplings, the scheme turns to be a four-level system with SGC. The spectrum of resonance fluorescence can be attributed to the SGC between the three upper dressed states. So the TQDs proposed here can give a feasible way to experimentally observe the effect of SGC, but without the need for near-degenerated states and nonorthogonal dipole moments.

The remainder of this paper is organized as follows. In Section 2, we describe the TQD model and calculate resonance fluorescence spectrum of the TQD system. In Section 3, we discussed the numerical results of the resonance fluorescence spectrum. Section 4 contains a summary and outlook.

2. Model and dynamic equations

We show the schematic of the band structure and level configuration of a TQD system in Fig. 1. At nanoscale interdot separation, the hole states are localized in the QDs and the electron states are rather delocalized. As shown in Fig. 1(a), in the absence of a gate voltage, the conduction-band electron levels are out of resonance and the electron tunneling between the QDs is very weak. In contrast, in the presence of a gate voltage, the conduction-band electron levels come close to resonance and the electron tunneling between the QDs is greatly enhanced, as shown in Fig. 1(b). In such system, the tunneling can be controlled by placing a gate electrode between the neighboring dots. And in the latter case the hole tunneling can be neglected because of the more off-resonant valence-band energy levels. Thus we can give the schematic of the level configuration of a TQD system, as shown in Fig. 1(c). Without the excitation of the laser, no excitons are inside all QDs, which corresponds to state $|0\rangle$. When a laser field is applied, a direct exciton is created inside the QD1, condition represented by the state $|1\rangle$. Under the tunneling couplings, the electron can tunnel from QD1 to the QD2, and from QD2 to QD3. And we denote these indirect excitons as state $|2\rangle$ and state $|3\rangle$, respectively.

In the interaction picture and the rotating wave and dipole approximations, the Hamiltonian of this system is (we use units such that $\hbar = 1$)

$$H = \sum_{j=0}^{3} E_j |j\rangle\langle j| + [(\Omega_c e^{-i\omega_c t}|0\rangle\langle 1| + T_1|2\rangle\langle 1| + T_2|3\rangle\langle 2|) + H.c.], \quad (1)$$

where $E_j = \hbar\omega_j$ is the energy of state $|j\rangle$, ω_c is the laser frequency, $\Omega_c = \boldsymbol{\mu}_{01} \times \mathbf{e} \times E$ is the Rabi frequency of the transition $|0\rangle \rightarrow |1\rangle$, with $\boldsymbol{\mu}_{01}$ being the associated dipole transition-matrix element, $\mathbf{e}$ the polarization vector and E the electric-field amplitude of the laser pulse. And T_1 and T_2 are the tunneling coupling.

From the Liouville equation, we obtain the following equations for the density-matrix elements:

$$\dot{\rho}_{01} = i[\Omega_c(\rho_{11} - \rho_{00}) - T_1\rho_{02}] + \frac{1}{2}(2i\delta_1 - \Gamma_{10} - \gamma_1)\rho_{01}, \quad (2a)$$

$$\dot{\rho}_{02} = i(\Omega_c\rho_{12} - T_1\rho_{01} - T_2\rho_{03}) + \frac{1}{2}[i(\delta_1 + \delta_2) - \Gamma_{20} - \gamma_2]\rho_{02}, \quad (2b)$$

$$\dot{\rho}_{03} = i(\Omega_c\rho_{13} - T_2\rho_{02}) + \frac{1}{2}[i(\delta_1 + \delta_3) - \Gamma_{30} - \gamma_3]\rho_{03}, \quad (2c)$$

$$\dot{\rho}_{11} = i[\Omega_c(\rho_{01} - \rho_{10}) + T_1(\rho_{21} - \rho_{12})] - \Gamma_{10}\rho_{11}, \quad (2d)$$

$$\dot{\rho}_{12} = i[T_1(\rho_{22} - \rho_{11}) + \Omega_c\rho_{02} - T_2\rho_{13}] + \frac{1}{2}[i(\delta_1 - \delta_2) - \Gamma_{10} - \Gamma_{20} - \gamma_1 - \gamma_2]\rho_{12}, \quad (2e)$$

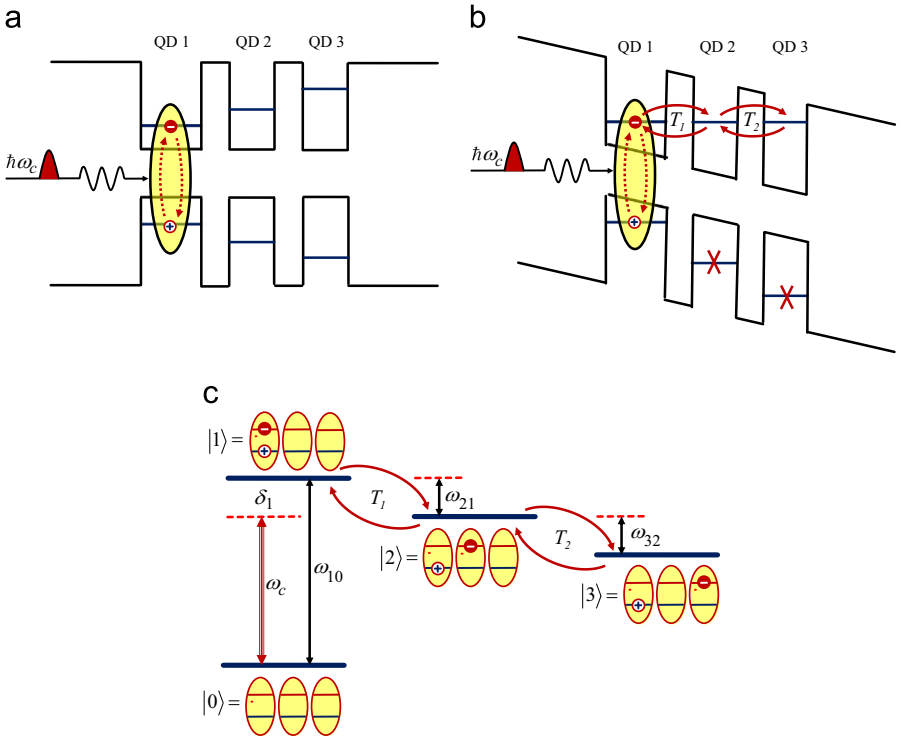

Fig. 1. (a) The schematic of band structure in the absence of a gate voltage. (b) The schematic of band structure in the presence of a gate voltage. (c) The schematic of the level configuration of a TQD system. (For interpretation of the references to color in this figure legend, the reader is referred to the web version of this article.)

$$\dot{\rho}_{13} = i[\Omega_c\rho_{03} + T_1\rho_{23} - T_2\rho_{12}] + \frac{1}{2}[i(\delta_1 - \delta_3) - \Gamma_{10} - \Gamma_{30} - \gamma_1 - \gamma_3]\rho_{13}, \tag{2f}$$

$$\dot{\rho}_{22} = iT_1(\rho_{12} - \rho_{21}) + iT_2(\rho_{32} - \rho_{23}) - \Gamma_{20}\rho_{22}, \tag{2g}$$

$$\dot{\rho}_{23} = i[T_2(\rho_{33} - \rho_{22}) + T_1\rho_{13}] + \frac{1}{2}[i(\delta_2 - \delta_3) - \Gamma_{20} - \Gamma_{30} - \gamma_2 - \gamma_3]\rho_{23}, \tag{2h}$$

$$\dot{\rho}_{33} = iT_2(\rho_{23} - \rho_{32}) - \Gamma_{30}\rho_{33}, \tag{2i}$$

$$\dot{\rho}_{ij} = -\dot{\rho}_{ji}^{*}, \tag{2j}$$

$$\rho_{00} + \rho_{11} + \rho_{22} + \rho_{33} = 1. \tag{2k}$$

Here the detunings are defined as $\delta_1 = (\omega_{01} - \omega_c)$, $\delta_2 = \delta_1 + 2\omega_{21}$ and $\delta_3 = \delta_1 + 2\omega_{21} + 2\omega_{31}$, with ω_{mn} the transition frequency between $|m\rangle$ and $|n\rangle$ states. And Γ_{10}, Γ_{20} and Γ_{30} are the radiative decay rates of populations from $|1\rangle \to |0\rangle$, $|2\rangle \to |0\rangle$ and $|3\rangle \to |0\rangle$, and γ_1, γ_2 and γ_3 are the pure dephasing rates. And we denote $\Gamma_1 = \Gamma_{10} + \gamma_1$, $\Gamma_2 = \Gamma_{20} + \gamma_2$ and $\Gamma_3 = \Gamma_{30} + \gamma_3$ as the effective parameters.

Following the common method used in Ref. [15] and [33], we calculate the steady-state fluorescence spectrum. As is well known, the fluorescence spectrum is proportional to the Fouriertransform of the steady-state correlation function $\lim_{t\to\infty}\langle E^{(-)}(r, \tau + t) \times E^{(+)}(r, t)\rangle$ [37], where $E^{(\pm)}(r, t)$ are the positive and negative frequency parts of the radiation field in the far zone, which consists of a free field operator, and a source-field operator that is proportional to the atomic polarization operator. Thus the incoherent fluorescence spectrum $S(\omega)$ can be expressed in terms of the atomic correlation function

$$S(\omega) = \mathrm{Re}\int_0^\infty \lim_{t\to\infty}\langle \Delta D^{+}(\tau + t) \times \Delta D^{-}(t)\rangle e^{-i\omega t} d\tau, \tag{3}$$

where Re denotes the real part, and $\Delta D^{\pm}(t) = \Delta D^{\pm}(t) - \langle \Delta D^{\pm}(\infty)\rangle$ is the deviation of the dipole polarization operator $D^{\pm}(t)$ from its mean steady-state value, and

$$D^{+}(t) = \mu_{01} a_1^{\dagger} a_2, \tag{4a}$$

$$D^{-}(t) = [D^{+}(t)]^{\dagger}. \tag{4b}$$

Then we rewrite Eqs. (2a–2k) in the form

$$\frac{d}{dt}\mathbf{\Psi} = L\mathbf{\Psi} + \mathbf{I}, \tag{5}$$

where $\mathbf{\Psi} = (\rho_{01}, \rho_{02}, \rho_{03}, \rho_{10}, \rho_{11}, \rho_{12}, \rho_{13}, \rho_{20}, \rho_{21}, \rho_{22}, \rho_{23}, \rho_{30}, \rho_{31}, \rho_{32}, \rho_{33})^T$, and $\mathbf{L}$ is a 15×15 matrix. The elements of $\mathbf{L}$ and $\mathbf{I}$ can be found explicitly from Eqs. (2a–2k).

By means of the quantum regression theorem [38,39], the steady spectrum of the fluorescence spectrum from the state $|1\rangle$ to the ground state $|0\rangle$ can be obtained

$$S(\delta_k) = \mathrm{Re}\left\{M_{11}\bar{\rho}_{11} + M_{12}\bar{\rho}_{12} + M_{13}\bar{\rho}_{13} + \sum_l N_{1l} I_l \bar{\rho}_{10}\right\}, \tag{6}$$

where

$$M_{ij} = [(z - L)^{-1}|_{z = i\delta_k}]_{i,j}, N_{ij} = [L^{-1}(z - L)^{-1}|_{z = i\delta_k}]_{i,j}. \tag{7}$$

$\bar{\rho}_{ij}$ is the steady-state population ($i = j$) and atomic coherence ($i \neq j$), which can be obtained by setting $\dot{\rho}_{ij} = 0$ and solving numerically Eq. (2a–2k). δ_k is the detuing between the fluorescence and the transition $|1\rangle \to |0\rangle$. In the next part, we will calculate the corresponding fluorescence spectrum by tuning the coupling of the tunneling. And this parameter depends on the barrier characteristics and the external electric field.

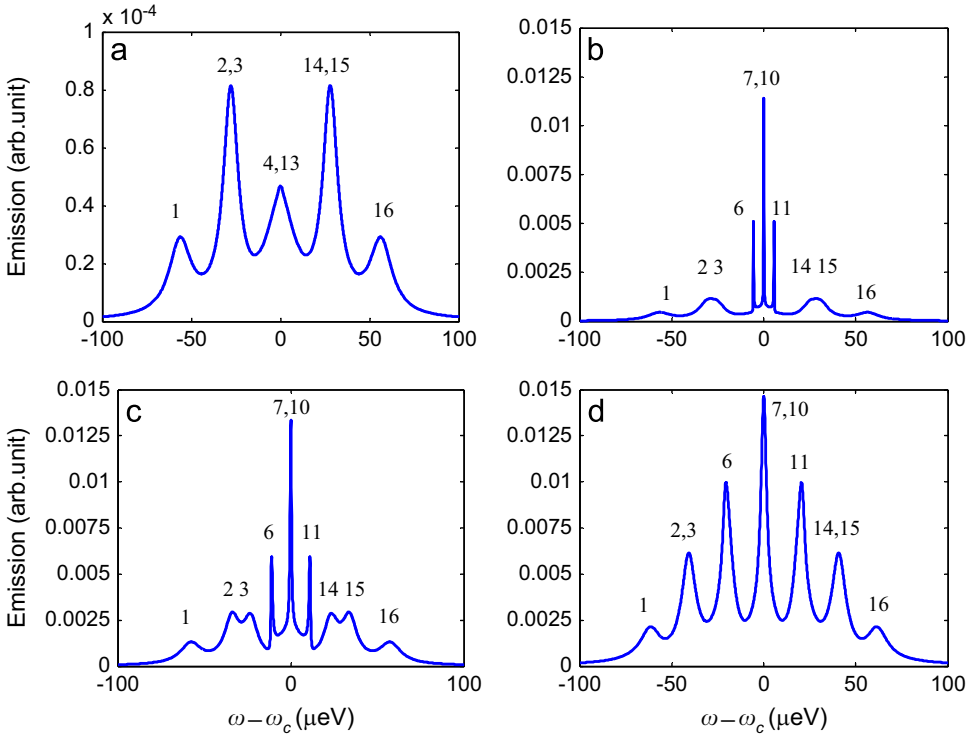

Fig. 2. Calculated spectrum of resonance fluorescence for fixed value of $T_1 = 20$ μeV and different value of T_2: (a) $T_2 = 0$, (b) $T_2 = 4$ μeV, (c) $T_2 = 8$ μeV, (d) $T_2 = 16$ μeV. The other parameters are $\Omega_c = 20$ μeV, $\delta_1 = 0$, $\omega_{21} = \omega_{32} = 0$, $\Gamma_{10} = 6.6$ μeV, $\Gamma_{20} = \Gamma_{30} = 10^{-4}\Gamma_{10}$, $\Gamma_1 = 20$ μeV, $\Gamma_2 = \Gamma_3 = 10^{-3}\Gamma_1$. The number in Fig. 2 denotes the peaks originate from which transition in Fig. 3(a). (For interpretation of the references to color in this figure legend, the reader is referred to the web version of this article.)

3. Results and discussions

For our investigation, we assume that the radiative decay rate of populations $\Gamma_{10} \simeq 6.6$ μeV [40], $\Gamma_{20} = \Gamma_{30} \simeq 10^{-4}\Gamma_{10}$ [41], and the effective dephasing parameters, $\Gamma_1 \simeq 20$ μeV [42], $\Gamma_2 = \Gamma_3 \simeq 10^{-3}\Gamma_1$ [43]. The tunneling couplings can be controlled by the barrier characteristics and the external electric field. We mainly focus on the case of $\delta_1 = \omega_{21} = \omega_{32} = 0$.

First, we fix the value of Ω_c and T_1 to 20 μeV, and show the results in Fig. 2 for different value of T_2. When $T_2 = 0$, which means the electron can tunnel from QD 1 to the QD 2, but cannot tunnel from QD 2 to QD 3. Thus the system is like a double QD system and five bored peaks appear in the spectrum (Fig. 2(a)). And the height of the middle peak is lower than the inner bands. When the tunneling coupling T_2 is increased to 4 μeV, therefore three QDs are coupled together by the two tunneling couplings, as can be seen from Fig. 2(b) that three narrow peaks appear in the middle of the spectrum. And the height of these middle peaks is larger than the sidebands. Then when $T_2 = 8$ μeV, the intensity of the three narrow peaks in the middle is increased, as well as the splittings between these peaks (Fig. 2(c)). When we increase the tunneling coupling to $T_2 = 16$ μeV, the width of the three peaks in the middle are in the same order as those of the other peaks, while the height of the peaks continue to increase (Fig. 2(d)).

It is well known that positions, heights, and widths of the fluorescence peaks are determined by the energies, steady-state populations, and electronic dipole moments of dressed states. In order to interpret the above numerical results, we investigate the properties of the dressed states. Under the resonant coupling of the laser field and the tunneling, the energy eigenvalues of these dressed states [44] can be written as follows:

$$\lambda_4 = -\lambda_1 = \kappa_+, \tag{8a}$$

$$\lambda_3 = -\lambda_2 = \kappa_-, \tag{8b}$$

where

$$\kappa_\pm = \sqrt{\frac{(\Omega_c{}^2 + T_1{}^2 + T_2{}^2) \pm \sqrt{(\Omega_c{}^2 + T_1{}^2 + T_2{}^2)^2 - 4\Omega_c{}^2 T_2{}^2}}{2}}. \tag{9}$$

Then the dressed states can be express as

$$|\Psi_1\rangle = C_{10}|0\rangle + C_{11}|1\rangle + C_{12}|2\rangle + C_{13}|3\rangle, \tag{10a}$$

$$|\Psi_2\rangle = -C_{20}|0\rangle + C_{21}|1\rangle - C_{22}|2\rangle + C_{23}|3\rangle, \tag{10b}$$

$$|\Psi_3\rangle = -C_{30}|0\rangle + C_{31}|1\rangle - C_{32}|2\rangle + C_{33}|3\rangle, \tag{10c}$$

$$|\Psi_4\rangle = C_{40}|0\rangle + C_{41}|1\rangle + C_{42}|2\rangle + C_{43}|3\rangle, \tag{10d}$$

where

$$C_{i0} = \frac{1}{D_i}\frac{\Omega_c(\lambda_i{}^2 - T_2{}^2)}{T_1 T_2 \lambda_i}, \tag{11a}$$

$$C_{i1} = \frac{1}{D_i}\frac{\lambda_i{}^2 - T_2{}^2}{T_1 T_2}, \tag{11b}$$

$$C_{i2} = \frac{1}{D_i}\frac{\lambda_i}{T_2}, \tag{11c}$$

$$C_{i3} = \frac{1}{D_i}, \tag{11d}$$

$$D_i = \sqrt{1 + \left(\frac{\lambda_i}{T_2}\right)^2 + \left(\frac{\lambda_i{}^2 - T_2{}^2}{T_1 T_2}\right)^2 + \left(\frac{\Omega_c(\lambda_i{}^2 - T_2{}^2)}{T_1 T_2 \lambda_i}\right)^2}. \tag{11e}$$

and Eqs. (10a–10d) can be written in the form

$$|\Psi_i\rangle = \sum C_{ik}|k\rangle \times \ (i = a, b, c, d;\ k = 0, 1, 2, 3) \tag{12}$$

Therefore both the state $|1\rangle$ and the state $|0\rangle$ (see Fig. 1(a)) are split into four dressed states (see Fig. 3(a)), which are $|\Psi_1\rangle$, $|\Psi_2\rangle$, $|\Psi_3\rangle$ and $|\Psi_4\rangle$ for the bare-state state $|1\rangle$, while $|\Psi_1{}'\rangle$, $|\Psi_2{}'\rangle$, $|\Psi_3{}'\rangle$ and $|\Psi_4{}'\rangle$ for the bare-state state $|0\rangle$. And the fluorescence from the state $|1\rangle$ to the ground state $|0\rangle$ has 16 dipole transitions in the dressed-state representation. (Every dipole transition is numbered in Fig. 3(a)). Note that though $|\Psi_i\rangle$ and $|\Psi_i{}'\rangle$ are different in constant energy by the energy difference between state $|1\rangle$ and $|0\rangle$, the dressed states $|\Psi_i\rangle$ has the same expressions and the eigenvalues as the dressed states $|\Psi_i{}'\rangle$ with $i = 1, 2, 3, 4$.

In order to give an explicit explanation of the fluorescence spectrum, we fix the Rabi frequency of the laser field Ω_c and the tunneling coupling T_1 at $\Omega_c = T_1 = 20$ μeV, and show the dressed-state eigenvalues and corresponding populations as functions of the other tunneling coupling T_2 (see Fig. 4(a) and (b)). It is obvious that the eigenvalues λ_1 and λ_4 depend weakly on T_2, while λ_2 and λ_3 are significantly affected by T_2. The populations of $|\Psi_1\rangle$, $|\Psi_2\rangle$, $|\Psi_3\rangle$ and $|\Psi_4\rangle$ are also influenced by T_2, and all the four dressed states are well populated.

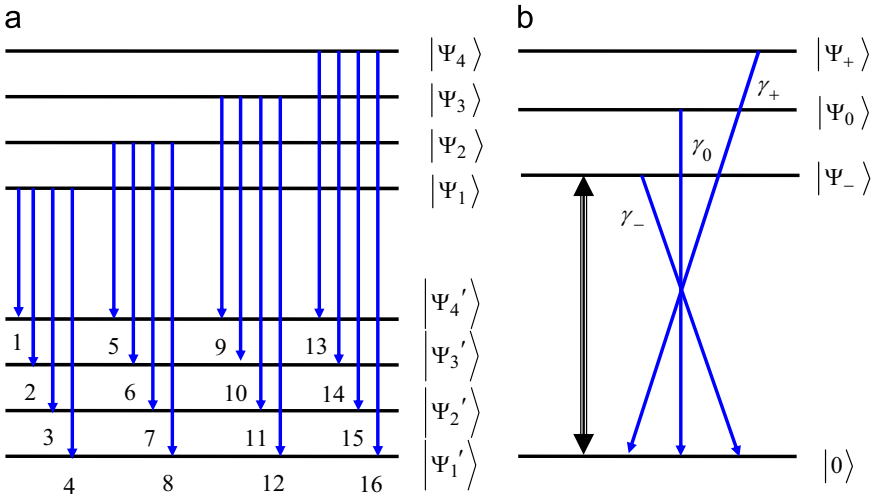

Fig. 3. (a) Dressed-state under the coupling of the laser field and tunneling. And dipole transitions are numbered from 1 to 16. (b) Dressed-state under the two tunneling couplings. And the interference occurs from the three decay channels $|\Psi_0\rangle \to |0\rangle$, $|\Psi_+\rangle \to |0\rangle$ and $|\Psi_-\rangle \to |0\rangle$. (For interpretation of the references to color in this figure legend, the reader is referred to the web version of this article.)

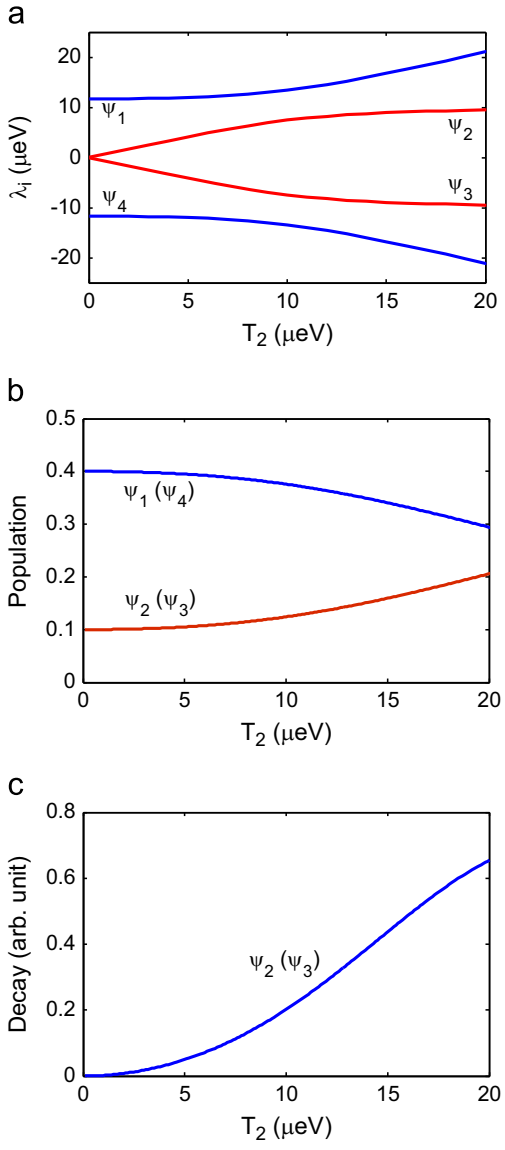

Fig. 4. Properties of dressed states as functions of the tunneling coupling T_2: (a) the eigen energies λ_i, (b) steady-state populations of the dressed state $|\Psi_i\rangle$, (c) decay rates of the dressed state $|\Psi_2\rangle$ and $|\Psi_3\rangle$. Other parameters are the same as those in Fig. 2. (For interpretation of the references to color in this figure legend, the reader is referred to the web version of this article.)

As we know that the decay rate of the transition between the dressed state $|\Psi_i\rangle$ to $|\Psi_j'\rangle$ is proportional to the squared dipole moments $R_{ij}=|\langle j|\mathbf{P}|i\rangle|^2$, where $\mathbf{P}=\boldsymbol{\mu}_{01}|0\rangle\langle 1|$ is the transition dipole moment operator between $|0\rangle$ and $|1\rangle$ in the bare state basis. R_{ij} can be calculated with the expression

$$R_{ij}=|\langle j|\mathbf{P}|i\rangle|^2=|C_{j0}|^2\boldsymbol{\mu}_{01}{}^2|C_{i1}|^2\times(i,j=1,2,3,4) \tag{13}$$

We can interpret the numerical results in Fig. 2 with the energies, populations and decay rates of the dressed states. The triple peaks in the middle originate from the transitions 6, 7, 10 and 11 (Fig. 2(b) and (c)). When the value of the tunneling coupling T_2 is small, the decay rate of the state $|\Psi_2\rangle$ and $|\Psi_3\rangle$ is much smaller than those of the state $|\Psi_1\rangle$ and $|\Psi_4\rangle$ (Fig. 4(c)). Therefore the triple peaks in the middle are much narrower than the others. The energy space, populations and decay rates of the dressed state $|\Psi_2\rangle$ and $|\Psi_3\rangle$ grow with an increasing of T_2, which results in the increasing of splittings between the peaks, the heights and widths of the triple peaks in the middle.

The above results can also be viewed as the effect of SGC between the dressed states. In the dressed-state representation of the tunneling couplings T_1 and T_2, the system turns to be a four-level scheme with three close-lying excited states $|\Psi_0\rangle$, $|\Psi_+\rangle$ and $|\Psi_-\rangle$ (see Fig. 3(b)). In the resonant case, the energy eigenvalues of these dressed states are $\lambda_0=0$ and $\lambda_\pm=\pm\sqrt{T_1{}^2+T_2{}^2}$, and the corresponding eigenstates are

$$|\Psi_0\rangle=-\frac{T_2}{T}|1\rangle+\frac{T_1}{T}|3\rangle, \tag{14a}$$

$$|\Psi_+\rangle=\frac{1}{\sqrt{2}}\left(\frac{T_1}{T}|1\rangle-|2\rangle+\frac{T_2}{T}|3\rangle\right), \tag{14b}$$

$$|\Psi_-\rangle=\frac{1}{\sqrt{2}}\left(\frac{T_1}{T}|1\rangle+|2\rangle+\frac{T_2}{T}|3\rangle\right), \tag{14c}$$

where

$$T=\sqrt{T_1{}^2+T_2{}^2}. \tag{15}$$

It is clear that the properties of the dressed states, take energy positions as an example, are determined by the tunneling couplings T_1 and T_2. These three dressed states decay to the ground state $|0\rangle$ with rates $\gamma_0=\Gamma_{10}T_2{}^2/T^2$, $\gamma_+=\gamma_-=\Gamma_{10}T_1{}^2/2T^2$, respectively, and SGC arises from these three dressed states. When T_2 is relatively small compared with T_1, the SGC between the three spontaneous emission pathways $|\Psi_0\rangle\to|0\rangle$, $|\Psi_+\rangle\to|0\rangle$ and $|\Psi_-\rangle\to|0\rangle$ are so strong that sharp lines appears in the fluorescence spectrum (see Fig. 2(b) and (c)). When T_2 is large, the SGC between the spontaneous emission pathways are weaker, thus no linewidth narrowing occurs (see Fig. 2(d)).

From Eqs. (14a–14c), the properties of the dressed states $|\Psi_0\rangle$, $|\Psi_+\rangle$ and $|\Psi_-\rangle$ also depend on the tunneling coupling T_1. As a result, we can also anticipate the control of resonance fluorescence by changing the value of T_1. The numerical results are shown in Fig. 5, where the tunneling coupling T_2 is fixed at 10 μeV. We can also analyze the fluorescence spectrum in the dressed state picture of the three driving fields (see Fig. 3(a)). First, when $T_1=0$, the electron cannot tunnel from QD 1 to the QD 2 or from QD 2 to QD 3, which is like the case of single QD system. We can obtain Mollow-type resonance fluorescence spectrum shown in Fig. 5(a). When $T_1\neq 0$, we can see that three narrow peaks appear in the resonance fluorescence spectrum. With increasing value of T_1, the intensity of the three narrow peaks in the middle and the splittings between these peaks are increasing (Fig. 5(b)–(d)). Similar to the case in Fig. 2, the triple peaks in the middle are induced by the four transitions 6, 7, 10 and 11. The decay rates from the dressed states $|\Psi_2\rangle$ and $|\Psi_3\rangle$ decrease for a larger value of T_1. Therefore we can obtain three narrow peaks in the spectrum.

Keeping the properties of the dressed states $|\Psi_0\rangle$ and $|\Psi_\pm\rangle$ unchanged, we calculate the resonance fluorescence spectrum by tuning the Rabi frequency of the laser field, as shown in Fig. 6. When Ω_c is relatively small compared to that of the two tunneling coupling, i.e. $\Omega_c=1$ μeV, as can be seen that the spectrum consists of three peaks, whose widths are of the same order (see Fig. 6(a)). If all the three couplings are equal ($\Omega_c=T_1=T_2=10$ μeV), more peaks are obtained and with the middle peaks being higher than the sidebands (see Fig. 6(b)). When we increase the Rabi frequency to $\Omega_c=20$ μeV, nine peaks are obtained and three of them acquire linewidth narrowing. And the central peak becomes much larger than the other peaks (see Fig. 6(c)). When Ω_c is large enough, the nine emission peaks are well resolved (see Fig. 6(d)), and the narrowing of the three peaks are very prominent.

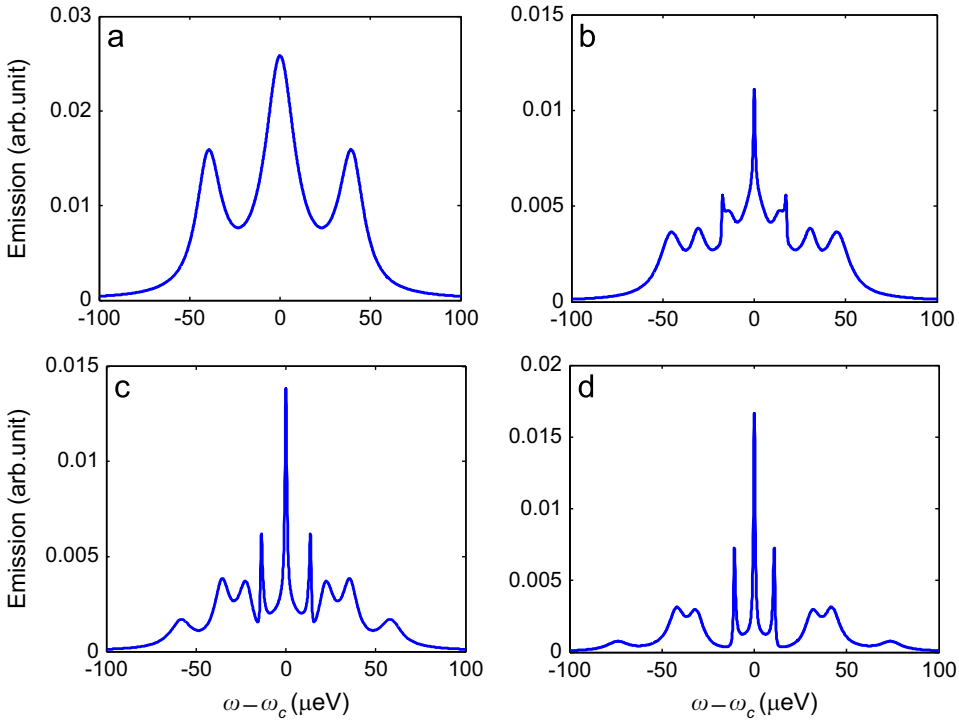

Fig. 5. Calculated spectrum of resonance fluorescence for fixed value of $T_2=10$ μeV and different value of T_1: (a) $T_1=0$, (b) $T_1=10$ μeV, (c) $T_1=20$ μeV, (d) $T_1=30$ μeV. Other parameters are the same as those in Fig. 2. (For interpretation of the references to color in this figure legend, the reader is referred to the web version of this article.)

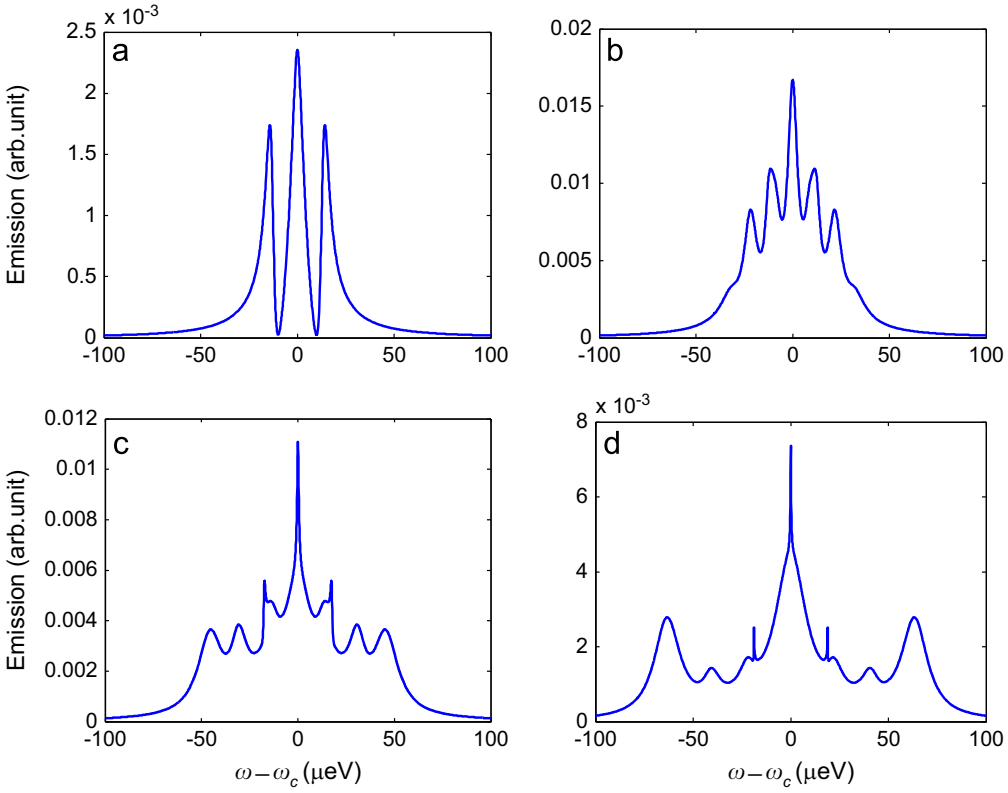

Fig. 6. Calculated spectrum of resonance fluorescence for fixed value of $T_1=20$ μeV, $T_2=20$ μeV, and different value of Ω_c: (a) $\Omega_c=1$ μeV, (b) $\Omega_c=10$ μeV, (c) $\Omega_c=20$ μeV, (d) $\Omega_c=30$ μeV. Other parameters are the same as those in Fig. 2. (For interpretation of the references to color in this figure legend, the reader is referred to the web version of this article.)

The above results can be seen clearly in the dressed state basis of all couplings (see Fig. 3(a)). In the case of $\Omega_c=1$ μeV, the states $|\Psi_2\rangle$ and $|\Psi_3\rangle$ (also $|\Psi_2'\rangle$ and $|\Psi_3'\rangle$) are near degenerate, and we can only see three broad peaks (see Fig. 6(a)). The decay of the transitions 1 and 16 are too weak to be observed, while the other 14 transitions shown in Fig. 3(a) contribute to the emission peaks.

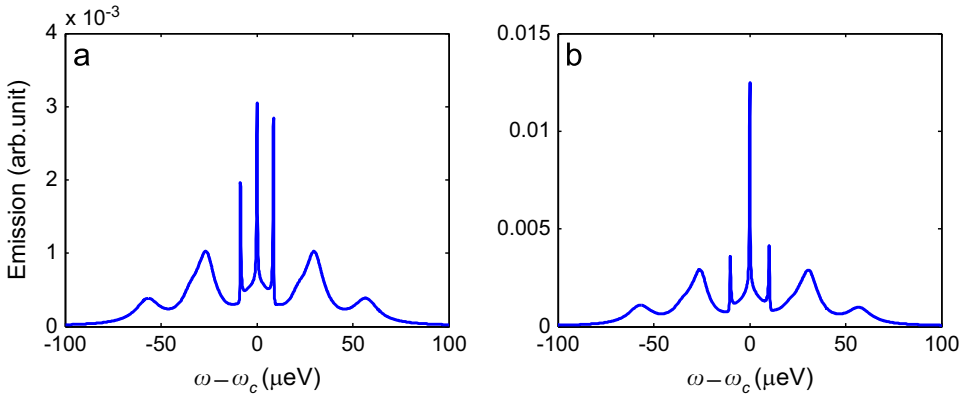

Fig. 7. Calculated spectrum of resonance fluorescence for fixed value of $T_1 = 20$ μeV, $T_2 = 20$ μeV, $\Omega_c = 10$ μeV, and different value of ω_{21} and ω_{32}: (a) $\omega_{21} = 0$, $\omega_{32} = 5$ μeV, (b) $\omega_{21} = -5$ μeV, $\omega_{32} = 10$ μeV. Other parameters are the same as those in Fig. 2. (For interpretation of the references to color in this figure legend, the reader is referred to the web version of this article.)

When Ω_c is increased to 10 μeV (see Fig. 6(b)), all the 16 transitions contribute to the spectrum. As the decay rates from the dressed states $|\Psi_2\rangle$ and $|\Psi_3\rangle$ are of the order of spontaneously decay rate, we get only broad peaks. When we further increase the value of Ω_c, the decay rates from the dressed states $|\Psi_2\rangle$ and $|\Psi_3\rangle$ are decreased. Therefore we observe narrow lines in the resonance fluorescence spectrum (see Fig. 6(c) and (d)).

In the above discussions, we consider the case of $\omega_{21} = \omega_{32} = 0$. If $\omega_{21} \neq 0, \omega_{32} \neq 0$, it is difficult to write the expressions of the dressed states in the simple forms. While we can qualitatively infer that the energies, populations, and decaying rates of the dressed states are modified, the fluorescence spectrum changes accordingly. We show two representative examples in Fig. 7. The nonzero value of ω_{21} and ω_{32} lead to the asymmetry of the spectrum and break the degeneracy of the transitions between the dressed states. As a matter of fact, we can get as much as thirteen peaks in the fluorescence spectrum (not shown here) with proper parameters.

4. Conclusions and outlook

In this paper, we investigate the steady-state spectrum of resonant fluorescence from a TQD system. The spectrum can be controlled by the tunneling coupling and some interesting features such as controllable triple narrow peaks are obtained. We analyze the resonance fluorescence spectrum in the dressed state basis of the two tunneling couplings and the laser field. The phenomena can also be attributed to SGC between the close-lying levels in the dressed state picture of the two tunneling couplings.

As is well known, it is very difficult to realize SGC in real atomic system owing to the rigorous requirements. But in the TQD system, we can simulate SGC by the tunneling coupling. Thus by observation of linewidth narrowing of the fluorescence spectrum from the TQDs, the existence of SGC can be proved without the need for closely lying levels and parallel dipole moments. Such a system may open the way to study the SGC effect in QDMs, and can find applications in many fields such as lasing without inversion, quantum information and computation. And also the narrowing of the peaks can be used in high-precision metrology.

Acknowledgment

This work is supported by the financial support from the National Basic Research Program of China (Grant No. 2013CB933300), the National Natural Science Foundation of China (Grant No. 11304308 and 61176046), Jilin Provincial Natural Science Foundation (Grant No. 20140101203JC), and the Hundred Talents Program of Chinese Academy of Sciences.

References

[1] X. Xu, B. Sun, P.R. Berman, D.G. Steel, A.S. Bracker, D. Gammon, L.J. Sham, Science 317 (2007) 929.
[2] A. Muller, E.B. Flagg, P. Bianucci, X.Y. Wang, D.G. Deppe, W. Ma, J. Zhang, G.J. Salamo, M. Xiao, C.K. Shih, Phys. Rev. Lett. 99 (2007) 187402.
[3] H.S. Borges, L. Sanz, J.M. Villas-Bôas, A.M. Alcalde, Phys. Rev. B: Condens. Matter 81 (2010) 075322.
[4] J.E. Rolon, S.E. Ulloa, Phys. Rev. B: Condens. Matter 82 (2010) 115307.
[5] A.J. Ramsay, Semicond. Sci. Technol 25 (2010) 103001.
[6] D. Loss, D.P. DiVincenzo, Phys. Rev. A: At. Mol. Opt. Phys. 57 (1998) 120.
[7] P. Michler, A. Imamolu, M.D. Mason, P.J. Carson, G.F. Strouse, S.K. Buratto, Nature 406 (2000) 968.
[8] X.Q. Li, Y.W. Wu, D. Steel, D. Gammon, T.H. Stievater, D.S. Katzer, D. Park, C. Piermarocchi, L.J. Sham, Science 301 (2003) 809.
[9] N. Akopian, N.H. Lindner, E. Poem, Y. Berlatzky, J. Avron, D. Gershoni, Phys. Rev. Lett. 96 (2006) 130501.
[10] B.R. Mollow, Phys. Rev. 188 (1969) 1969.
[11] F. Schuda, C.R. Stroud Jr., M. Hercher, J. Phys. B: At. Mol. Opt. Phys. 7 (1974) L198.
[12] G. Wrigge, I. Gerhardt, J. Hwang, G. Zumofen, V. Sandoghdar, Nat. Phys 4 (2008) 60.
[13] A.N. Vamivakas, Y. Zhao, C.Y. Lu, M. Atatüre, Nat. Phys 5 (2009) 198.
[14] D.J. Gauthier, Y.F. Zhu, T.W. Mossberg, Phys. Rev. Lett. 66 (1991) 2460.
[15] S.C. Tian, C.L. Wang, C.Z. Tong, L.J. Wang, H.H. Wang, X.B. Yang, Z.H. Kang, J.Y. Gao, Opt. Exp 20 (2012) 23559.
[16] M. Bayer, P. Hawrylak, K. Hinzer, S. Fafard, M. Korkusinski, Z.R. Wasilewski, O. Stern, A. Forchel, Science 291 (2001) 451.
[17] G.J. Beirne, C. Hermannstädter, L. Wang, A. Rastelli, O.G. Schmidt, P. Michler, Phys. Rev. Lett. 96 (2006) 137401.
[18] Q.H. Xie, A. Madhukar, P. Chen, N.P. Kobayashi, Phys. Rev. Lett. 75 (1995) 2542.
[19] R. Songmuang, S. Kiravittaya, O.G. Schmidt, Appl. Phys. Lett. 82 (2003) 2892.
[20] G. Rainò, A. Salhi, V. Tasco, M. De Vittorio, A. Passaseo, R. Cingolani, M. De Giorgi, E. Luna, A. Trampert, J. Appl. Phys. 103 (2008) 096107.
[21] C. Hsieh, Y. Shim, M. Korkusinski, P. Hawrylak, Rep. Prog. Phys 75 (2012) 114501.
[22] J.A. Brum, P. Hawrylak, Superlatt. Microstruct 22 (1997) 431.
[23] D. Loss, D.P. DiVincenzo, Phys. Rev. A: At. Mol. Opt. Phys. 57 (1998) 120.
[24] M.A. Nielsen, E. Knill, R. Laflamme, Nature 396 (1998) 52.
[25] D.P. DiVincenzo, D. Bacon, J. Kempe, G. Burkard, K.B. Whaley, Nature 408 (2000) 339.
[26] M. Stopa, Phys. Rev. Lett. 88 (2002) 146802.
[27] A.D. Greentree, J.H. Cole, A.R. Hamilton, L.C.L. Hollenberg, Phys. Rev. B: Condens. Matter 70 (2004) 235317.
[28] C.H. Bennet, D.P. Divincenzo, Nature 404 (2000) 247.
[29] J.H. Wu, J.Y. Gao, Phys. Rev. A: At. Mol. Opt. Phys. 65 (2002) 063807.
[30] M. Bajcsy, S. Hofferberth, V. Balic, T. Peyronel, M. Hafezi, A.S. Zibrov, V. Vuletic, M.D. Lukin, Phys. Rev. Lett. 102 (2009) 203902.
[31] M.O. Scully, Phys. Rev. Lett. 104 (2010) 207701.
[32] O. Postavaru, Z. Harman, C.H. Keitel, Phys. Rev. Lett. 106 (2011) 033001.
[33] P. Zhou, S. Swain, Phys. Rev. Lett. 77 (1996) 3995.
[34] F.L. Li, S.Y. Zhu, Phys. Rev. A: At. Mol. Opt. Phys. 59 (1999) 2330.
[35] F.L. Li, S.Y. Gao, S.Y. Zhu, Phys. Rev. A: At. Mol. Opt. Phys. 67 (2003) 063818.
[36] M.A. Macovei, J. Phys. B: At. Mol. Opt. Phys. 40 (2007) 387.

[37] M.O. Scully, M.S. Zubairy, Quantum Optics, Cambridge University, London Press, 1997 (Chap. 10).
[38] M. Lax, Phys. Rev 172 (1968) 350.
[39] S. Swain, J. Phys. A: Gen. Phys. 14 (1981) 2577.
[40] P. Chen, C. Piermarocchi, L.J. Sham, Phys. Rev. Lett. 87 (2001) 067401.
[41] V. Negoita, D.W. Snoke, K. Eberl, Phys. Rev. B: Condens. Matter 60 (1999) 2661.
[42] P. Borri, W. Langbein, U. Woggon, M. Schwab, M. Bayer, Phys. Rev. Lett. 91 (2003) 267401.
[43] L.V. Butov, A. Zrenner, G. Abstreiter, G. Böhm, G. Weimann, Phys. Rev. Lett. 73 (1994) 304.
[44] C. Cohen-Tannoudji, J. Dupont-Roc, G. Grynberg, Atom–Photon Interactions, Wiley-VCH, Weinheim, 2004.